INTERNATIONAL JOURNAL FOR NUMERICAL METHODS IN FLUIDS
Int. J. Numer. Meth. Fluids 2004; **44**:1185–1205 (DOI: 10.1002/fld.680)

Using a piecewise linear bottom to fit the bed variation in a laterally averaged, z-co-ordinate hydrodynamic model

XinJian Chen*,†

Surface Water Improvement & Management Program, Southwest Florida Water Management District, 7601 Highway 301 North, Tampa, FL 33637, U.S.A.

SUMMARY

In developing a 3D or laterally averaged 2D model for free-surface flows using the finite difference method, the water depth is generally discretized either with the z-co-ordinate (z-levels) or a transformed co-ordinate (e.g. the so-called σ-co-ordinate or σ-levels). In a z-level model, the water depth is discretized without any transformation, while in a σ-level model, the water depth is discretized after a so-called σ-transformation that converts the water column to a unit, so that the free surface will be 0 (or 1) and the bottom will be -1 (or 0) in the stretched co-ordinate system. Both discretization methods have their own advantages and drawbacks. It is generally not conclusive that one discretization method always works better than the other. The biggest problem for the z-level model normally stems from the fact that it cannot fit the topography properly, while a σ-level model does not have this kind of a topography-fitting problem.

To solve the topography-fitting problem in a laterally averaged, 2D model using z-levels, a piecewise linear bottom is proposed in this paper. Since the resulting computational cells are not necessarily rectangular looking at the x–z plane, flux-based finite difference equations are used in the model to solve the governing equations. In addition to the piecewise linear bottom, the model can also be run with full cells or partial cells (both full cell and partial cell options yield a staircase bottom that does not fit the real bottom topography). Two frictionless wave cases were chosen to evaluate the responses of the model to different treatments of the topography. One wave case is a boundary value problem, while the other is an initial value problem. To verify that the piecewise linear bottom does not cause increased diffusions for areas with steep bottom slopes, a barotropic case in a symmetric triangular basin was tested. The model was also applied to a real estuary using various topography treatments. The model results demonstrate that fitting the topography is important for the initial value problem. For the boundary value problem, topography-fitting may not be very critical if the vertical spacing is appropriate. Copyright © 2004 John Wiley & Sons, Ltd.

KEY WORDS: piecewise linear bottom; topography-fitting; z-level model; full cell; partial cell; narrow rivers and estuaries; laterally averaged 2D models; free-surface correction method

1. INTRODUCTION

Twomethods are generally used to discretize the water column in a 3D or a laterally averaged 2D hydrodynamic model using the finite difference method. One is to discretize the

*Correspondence to: XinJian Chen, Surface Water Improvement & Management Program, Southwest Florida Water Management District, 7601 Highway 301 North, Tampa, FL 33637, U.S.A.
†E-mail: xinjian.chen@swfwmd.state.fl.us

Received 8 July 2003
Revised 19 November 2003

water column without any co-ordinate transformation, or the z-co-ordinate is directly used for the spatial discretization in the vertical direction. This kind of a hydrodynamic model is also called a z-level model. The other method is to discretize the water column after a co-ordinate transformation. One of the most popular co-ordinate transformations is the so-called σ-transformation that converts the water column to a unit, so that the free surface will be 0 (or 1) and the bottom will be -1 (or 0) in the stretched co-ordinate system. A hydrodynamic model that uses a σ-co-ordinate system is often called a σ-level model. In σ-level models (e.g. References [1, 2]), the water column is divided into a fixed number of vertical layers. The thickness of each layer can vary in the vertical direction but the ratio of the layer thickness to the total water depth is fixed for the same layer. Therefore, the layer thickness varies horizontally, depending on the water depth. A σ-co-ordinate model can fit the topography nicely but pays the price of pressure gradient errors and increased numerical diffusions for areas with steep bottom slopes [3, 4].

In a z-level model, the water column is sliced into different layers with horizontal planes. Although the vertical spacing may vary in the vertical direction, each layer has the same thickness everywhere. Model variables are placed at the same level for the same layer. Traditional z-level models use a relatively thick surface layer to cover the variation of the free surface [5], while recent z-level models allow the free surface to travel from one layer to another [6–10]. Depending on the water depth, the number of grid points in the vertical direction varies in a z-level model. Shallow areas have fewer vertical grid points than deep areas do. In most z-level models, if the bottom elevation is lower than the middle point of a layer, then the entire cell will be taken as a valid one and the bottom of the layer is the bottom boundary in the computational domain. Otherwise, the cell is abandoned and the top of the layer will be used as the bottom boundary. As a result of this treatment, the bottom cell in the computation always has the same thickness as the horizontal layer. This kind of a bottom cell is a full cell. Recent improvements of z-level models involved the use of partial cells for a better approximation of the bottom topography. Instead of using the thickness of the layer ($\Delta\zeta$), the difference between the top of the layer and the real physical bottom is used as the bottom cell thickness [10, 11], which is generally smaller than the layer thickness. Since the side view (looking at the x–z plane) of a full cell or a partial cell is rectangular, both bottom treatment methods yield a staircase bottom that does not fit the real topography. To eliminate the staircase bottom, this paper proposes the use of a piecewise linear bottom to fit the topography. Figure 1 shows the various treatment methods for the bottom topography. When a piecewise linear bottom is used, the side views of the bottom cells are generally not rectangular. Obviously, the piecewise linear bottom is terrain-following, while the full cell and partial cell methods are not. The piecewise linear bottom, along with the full cell and partial cell options, is implemented in a laterally averaged model named LAMFE [7–9, 12, 13], allowing some comparisons of model results using different topography treatment methods [13].

In the following sections, governing equations for hydrodynamics and transport processes in narrow rivers and estuaries are first given in Section 2. Details on the piecewise linear bottom are then described in Section 3, followed by a presentation of flux-based finite difference equations using a free-surface correction (FSC) method in Section 4. Section 5 presents several test cases to investigate responses of the model to various treatments of the bottom topography. Two frictionless wave cases were evaluated. One wave case is an initial value problem, while the other is a boundary value problem. The initial value problem is a seiche oscillation in a triangular basin and the boundary value problem is a co-oscillating long wave

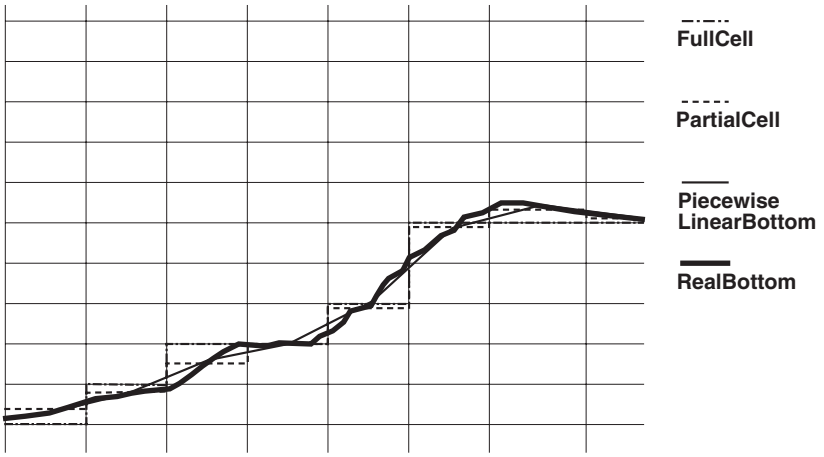

Figure 1. Various topography treatment methods in the laterally averaged, two-dimensional hydrodynamic model LAMFE.

in a channel with a small bottom slope. To verify that the piecewise linear bottom does not cause increased numerical diffusions for areas with steep bottom slopes, a barotropic case in a symmetric triangular basin was tested with a vertically varying salinity. The model was also applied to an actual narrow estuary using various bottom treatments. The conclusions of the study are summarized in Section 6.

2. GOVERNING EQUATIONS

A laterally averaged model for estuaries (LAMFE) has been developed to study hydrodynamics and transport processes in various narrow rivers and estuaries in the southwest portion of the Florida Peninsula [7, 9, 11–13]. The model solves the following laterally averaged, two-dimensional equations of hydrodynamics and transport processes:

$$\frac{\partial ub}{\partial x} + \frac{\partial wb}{\partial z} = v \tag{1}$$

$$\frac{\partial u}{\partial t} + u\frac{\partial u}{\partial x} + w\frac{\partial u}{\partial z} = -\frac{\tau_{wx}}{\rho b} - \frac{1}{\rho}\frac{\partial p}{\partial x} + \frac{1}{\rho b}\frac{\partial}{\partial x}\left(\rho b A_h \frac{\partial u}{\partial x}\right) + \frac{1}{\rho b}\frac{\partial}{\partial z}\left(\rho b A_v \frac{\partial u}{\partial z}\right) \tag{2}$$

$$p = g\int_z^\eta \rho \, \mathrm{d}z \tag{3}$$

$$b\frac{\partial c}{\partial t} + \frac{\partial ubc}{\partial x} + \frac{\partial wbc}{\partial z} = \frac{\partial}{\partial x}\left(bB_h \frac{\partial c}{\partial x}\right) + \frac{\partial}{\partial z}\left(bB_v \frac{\partial c}{\partial z}\right) + vc_t \tag{4}$$

where t is the time, x the longitudinal co-ordinate along the river/estuary, z the vertical co-ordinate, u and w denote velocity components in x- and z-directions, respectively; v is the lateral velocity from lateral inputs (sheet flow of direct runoff, tributary, etc.); b, p, g and η denote the width, pressure, gravitational acceleration and the free surface elevation, respectively; τ_{wx} represents the shear stress due to the friction acting on the sidewall ($=\rho C_w u[u^2+w^2]^{1/2}$, where C_w is a non-dimensional frictional coefficient for sidewalls); A_h and A_v are kinetic eddy viscosities in the x- and z-directions, respectively; c represents concentration (salt or temperature); c_t represents concentration in tributaries; B_h and B_v are eddy diffusivities in the x- and z-directions, respectively; and D is the density which is a function of salinity and temperature.

Replacing p in Equation (2) with the right-hand side of Equation (3) and using the Leibnitz integration law, the longitudinal pressure gradient in Equation (2) can be written as

$$\frac{\partial p}{\partial x} = g\rho_\eta \frac{\partial \eta}{\partial x} + g\int_z^\eta \frac{\partial \rho}{\partial x}\,\mathrm{d}z \tag{5}$$

where ρ_η represents density at the free surface. The first term on the right-hand side of Equation (5) is the barotropic pressure component, while the second term is the baroclinic pressure component. Inserting Equation (5) into Equation (2) and using the Bousinnesq approximation, one obtains

$$\frac{\partial u}{\partial t} + u\frac{\partial u}{\partial x} + w\frac{\partial u}{\partial z} = -\frac{C_w u}{b}\sqrt{u^2+w^2} - g\frac{\partial \eta}{\partial x} - \frac{g}{\rho}\int_z^\eta \frac{\partial \rho}{\partial x}\,\mathrm{d}z + \frac{1}{b}\frac{\partial}{\partial x}\left(bA_h\frac{\partial u}{\partial x}\right) + \frac{1}{b}\frac{\partial}{\partial z}\left(bA_v\frac{\partial u}{\partial z}\right) \tag{6}$$

The equation for the location of the free surface is obtained by integrating Equation (1) over the water depth. Considering the direct rainfall to the water surface in the model, we obtain

$$b_\eta\frac{\partial \eta}{\partial t} = -\frac{\partial}{\partial x}\int_{h_0}^\eta ub\,\mathrm{d}z + \int_{h_0}^\eta v\,\mathrm{d}z + rb_\eta \tag{7}$$

where h_0 is the bottom elevation, r the net rain intensity (rainfall minus evaporation) having the same units as the velocity and b_η the width of the river/estuary at the free surface.

The effect of the direct rainfall on the concentration distribution is considered as the flux to the top cell of the water column as follows:

$$\frac{\partial \delta\eta bc}{\partial t} + \frac{\partial ub\delta\eta c}{\partial x} = \left(wbc + B_v b\frac{\partial c}{\partial z}\right)_- + \frac{\partial}{\partial x}\left(B_h\delta\eta b\frac{\partial c}{\partial x}\right) + \delta\eta v c_t + rb_\eta c_r \tag{8}$$

where $\delta\eta$ is the thickness of the surface layer, the subscript '$-$' denotes the bottom of the top layer and c_r represents salinity in rainfall (0 by default).

Equations (7) and (8) suggest how boundary conditions for Equations (1) and (4) are specified at the free surface. The boundary condition for Equation (2) (or Equation (6)) at the free surface is determined by the wind shear stress in the x-direction. At the bottom, it is assumed that no fluxes of water and/or materials entering/leaving the water column through

the bed and that turbulence is fully developed so that a log-layer distribution of velocity can be used to calculate the bottom shear stress. In the longitudinal direction, boundary conditions at the upstream and downstream boundaries are specified with either the free-surface elevation or the vertical profile of the longitudinal velocity. Specifying the longitudinal velocity profile also implies that appropriate Neumann-type boundary conditions are used for pressure. As a special case, normal velocity is set to zero if one or both ends are closed (dead ends).

3. COMPUTATIONAL CELLS

A Cartesian grid system using hybrid cells shown in Figure 2 is used to develop the laterally averaged 2D model. In Figure 2, long dashed lines form a total of $N_x N_z$ grid cells, where N_x is the number of grids in the longitudinal direction and N_z is the number of vertical layers used to discretize the water column. Each grid cell is numbered at its centre with indexes i and k in the longitudinal and vertical directions, respectively. With a staggered arrangement of model variables, $u_{i,k}$ is defined at the centre of the right face of the cell, while $w_{i,k}$ is defined at the centre of the top face. The density $\rho_{i,k}$, concentration $c_{i,k}$, river width $b_{i,k}$ and pressure $p_{i,k}$ are defined at the centre of the cell. The surface elevation (η_i) and water depth (D_i) are defined at the centre of the longitudinal grid. The geometry of the estuary is defined by the river width at the centre of the grid cell. The thick solid line in Figure 2 represents the piecewise linear bottom. The solid line and the short dashed line near the top of the graph are the water surfaces at two time points, t_1 and t_2, respectively.

As shown in Figure 2, the longitudinal spacing Δx varies only with i, while the layer thickness $\Delta\zeta$ is constant for the same k-index. It should be pointed out that grid cells formed

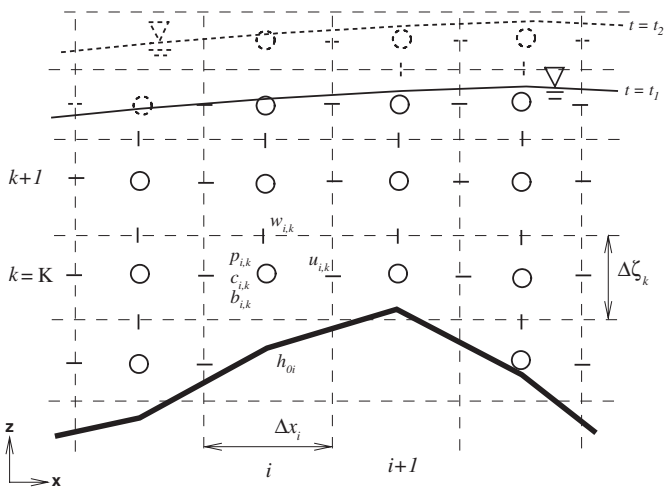

Figure 2. Discretizing the water column using z-levels with hybrid cells. The thick black line denotes the piecewise linear bottom. Long dashed lines form grid cells. The circle represents the pressure point, while '-' and '|' are u and w points, respectively. Concentrations, density and river width are defined at the pressure point. The solid line near the top of the graph is the water surface at a time point, while the short dashed line is the water surface at another time point.

by long dashed lines in Figure 2 are not necessarily the same as computational cells because of the longitudinal variations of the bed and water surface. Note that grid cells and computational cells are two different concepts in this context. The side views of grid cells are always rectangular, while computational cells are not necessarily rectangular looking from the side. Computational cells are the actual control volumes for which the governing equations are solved. Furthermore, owing to the staggered arrangement of model variables, computational cells (control volumes) for computing concentrations are not the same as those for computing the u-velocity even when they have the same cell indexes i and k. To distinguish computational cells for calculating the u-velocity from those for calculating concentrations, computational cells for calculating the u-velocity are called computational u-cells in this paper, while computational cells for computing concentrations are called computational c-cells.

In Figure 2, the water column with the longitudinal index of i has N_z grid cells, but has only three (3) computational c-cells stacked one on another at $t = t_1$. Denoting the k-indexes for the bottom and surface computational c-cells as kn_i and km_i, respectively, then $kn_i = K$ and $km_i = K + 2$. Obviously, only the middle computation c-cell (with the k-index $= K + 1$) is the same as the grid cell. Both the surface and bottom computational c-cells are not identical to their corresponding grid cells. At another time point ($t = t_2$), however, the water surface is higher than that at $t = t_1$ and the water column has four computational c-cells, of which the two interior ones are the same as the grid cells. Owing to a higher surface elevation, the maximum k-index at $t = t_2$ becomes $km_i = K + 3$. The model calculates and saves km at each time step for all the longitudinal grids. The criterion for determining km_i is to see whether the water surface η_i is above or below the middle point of a certain grid cell. The water surface η_i should always be higher than the middle point of the km_ith grid cell for the ith longitudinal grid. If the free surface drops below the middle point of the km_ith grid cell from one time step to the next time step, then the surface computational c-cell is aggregated to the cell below it. In this case, km_i is reduced by 1, so that η_i at the new time step is higher than the middle point of the km_ith grid cell. On the other hand, if a surface computational c-cell contains two ρ points (two grid cell centres) at a new time step, it is split into two computational c-cells. In this case, the top one is the new surface computational c-cell at the new time step and km_i is increased by 1. By implementing this kind of volume of fluid (VOF) technique, the free surface can travel from one layer to another and there is no need to use a thick surface layer to cover the free-surface variation. Therefore, thin layers can be used near the free surface, allowing a fine resolution for area near the water surface.

As can be seen in Figure 2, bottom computational u- and c-cells generally consist of one or more bottom grid cells that are directly adjacent to the bed. If more than one grid cell is involved, then only one grid cell centre is contained in the computational cell, with other grid cell centres being chopped off by the bed. To ensure that the bottom u-point is within the log-layer, the distance between the bottom u-point and the bed should be larger than the thickness of the viscous sub-layer. If the vertical distance between the lowest calculated u-velocity and the bed is smaller than the viscous sub-layer, the bottom computational u-cell is aggregated to the one above it to form a new bottom computational u-cell. Figure 3 shows the side view and the three-dimensional view of a typical bottom computational u-cell. The side and the three-dimensional views of a typical bottom computational c-cell are illustrated in Figure 4. Owing to the way the river width is defined, the shape of a bottom computational u-cell can be either an octahedron or a decahedron. For the computational c-cell, it can have 12, 13 or even 14 faces.

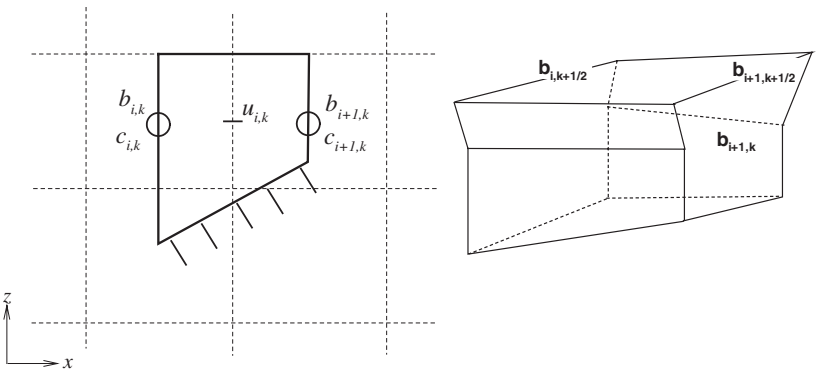

Figure 3. A side view (left) and a 3D view (right) of a typical bottom computational u-cell. The cell is an octahedron, but can also be a decahedron.

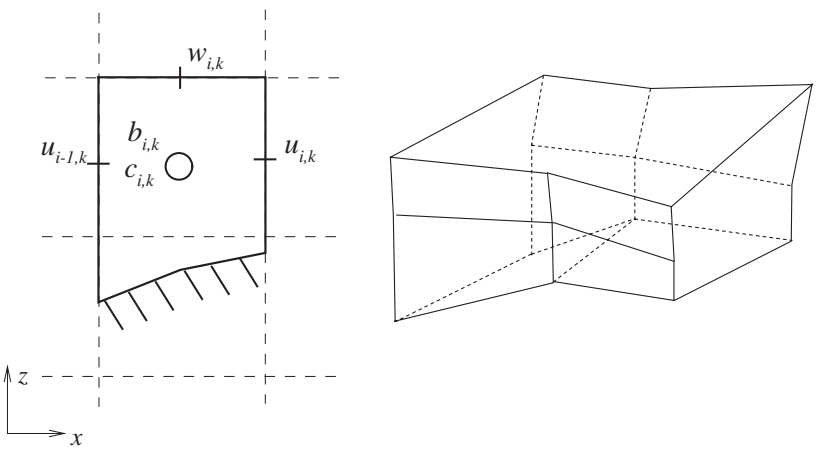

Figure 4. A side view (left) and a 3D view (right) of a typical bottom computational c-cell. Owing to the way the river width is defined, the cell generally has 13 faces.

4. NUMERICAL SCHEME

The model employs the FSC method described in Reference [12] to solve the momentum and continuity equations in two steps. In the first step, an intermediate longitudinal velocity is calculated with the explicit surface elevation gradient, before an intermediate free-surface elevation is estimated. In the second step, the intermediate velocity field is corrected to obtain the final velocity field, after a free-surface correction equation is solved to find the final free-surface elevation. The FSC method is an efficient method because it is unconditionally stable with respect to gravity waves, the vertical eddy viscosity term and the bottom and sidewall stresses. Details on the FSC method are documented in Reference [12]. This section presents the finite difference equations without any derivations of the FSC method.

The LAMFE model takes advantage of both the finite difference method and the finite volume method. For interior computational cells, because they are the same as their corresponding grid cells, the finite difference equation for the longitudinal momentum balance is directly derived from the partial differential equation (Equation (6)) with the implicit discretization of the vertical eddy viscosity term, but with the explicit discretization of the barotropic term

$$\frac{u_{i,k}^{n+*}-u_{i,k}^{n}}{\Delta t}=H_x^n-g\frac{\partial \eta^n}{\partial x}-\frac{C_w}{b_{i+1/2,k}}u_{i,k}^{n+*}\sqrt{(u_{i,k}^n)^2+(w_{i+1/2,k-1/2}^n)^2}$$

$$+\frac{1}{b_{i+1/2,k}}\frac{\partial}{\partial z}\left(bA_v\frac{\partial u^{n+*}}{\partial z}\right)_{i+1/2,k} \tag{9}$$

where Δt is the time step used in the computation; the superscript n represents the previous time step, while the superscript $n+^*$ represents the intermediate solution at the new time step; η^n is the free surface location at the previous time step; and H_x^n is an explicit finite difference operator containing the convection terms, the baroclinic term and the longitudinal eddy viscosity term.

For the bottom and surface computational cells, because they are generally different from their corresponding grid cells, the following flux-based finite difference equation is used to calculate the intermediate velocity:

$$\frac{u_{\mathrm{cc}}^{n+*}-u_{\mathrm{cc}}^{n}}{\Delta t}=\frac{G_x^n}{\rho V_{i+1/2,k}^n}-g\frac{\partial \eta^n}{\partial x}-\frac{\Delta x_i \Delta z_{i+1/2,k}^n}{V_{i+1/2,k}^n}C_w u_{i,k}^{n+*}\sqrt{(u_{i,k}^n)^2+(w_{i+1/2,k-1/2}^n)^2}$$

$$+\frac{1}{V_{i+1/2,k}^n}\left[\left(a_x A_h\frac{\partial u^n}{\partial x}\right)_{i+1,k}-\left(a_x A_h\frac{\partial u^n}{\partial x}\right)_{i,k}\right.$$

$$\left.+\left(a_z A_v\frac{\partial u^{n+*}}{\partial z}\right)_{i+1/2,k+1/2}-\left(a_z A_v\frac{\partial u^{n+*}}{\partial z}\right)_{i+1/2,k-1/2}\right] \tag{10}$$

where G_x^n represents the sum of the fluxes of the longitudinal momentum entering the computational u-cell plus the total baroclinic force acting on it; a_z is the projection of the area of the top/bottom face of the computational cell onto the horizontal plane; a_x is the area of the left/right face of the computational cell; Δz is the average cell thickness; and V is the volume of the cell. The left-hand side of the above equation represents the local acceleration at the centre of the computational u-cell. As a first order approximation, the local acceleration at the centre of the computational u-cell is related to that at the u-point as follows:

$$\left.\frac{\partial u}{\partial t}\right|_{\mathrm{cc}}=\left.\frac{\partial u}{\partial t}\right|_{\mathrm{up}}+\nabla\left(\left.\frac{\partial u}{\partial t}\right|_{\mathrm{up}}\right)\cdot\delta\boldsymbol{l} \tag{11}$$

where subscripts 'cc' and 'up' denote the cell centre and the u-point of the computational u-cell, respectively; ∇ denotes the divergence operator; and $\delta\boldsymbol{l}$ is a vector pointing from the u-point to the centre of the computational u-cell: $\delta\boldsymbol{l}=\delta x\boldsymbol{i}+\delta z\boldsymbol{k}$, where δx and δz are the

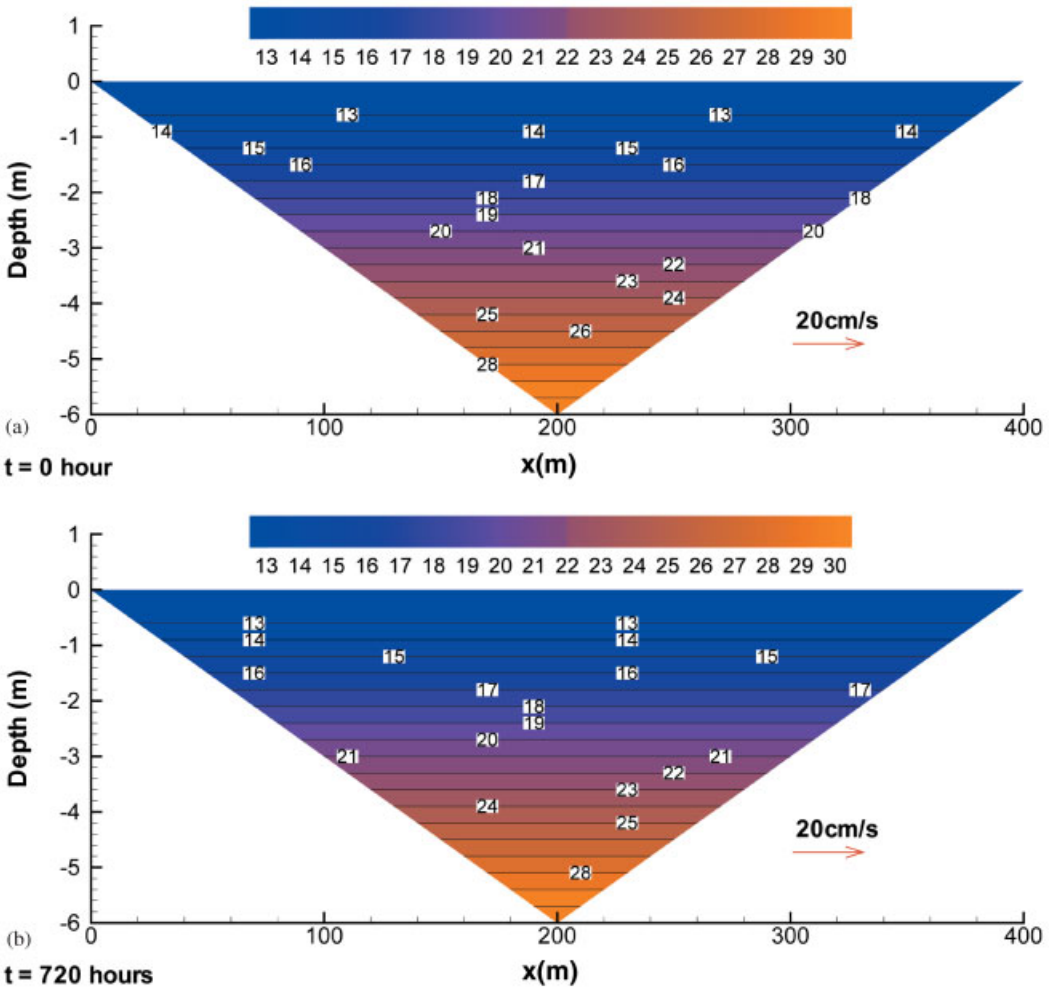

Plate 1. A symmetric triangular basin is filled with water that has a vertical salinity distribution at $t = 0$ h (a). The same salinity distribution is still retained without any artificial baroclinic circulation after the model was run for a simulation time period of 720 h (b). The piecewise linear bottom was used in the simulation.

projections of the distance between u-point and the centre of the cell in the x- and z-directions, respectively.

For shallow water flows in narrow rivers and estuaries, the vertical length scale is generally two to three orders of magnitude smaller than the longitudinal length scale and δx is insignificant in comparison with the longitudinal spacing. Therefore, the change of the local longitudinal acceleration of the water particle due to δx is negligible, or

$$\left.\frac{\partial u}{\partial t}\right|_{cc} \cong \left.\frac{\partial u}{\partial t}\right|_{up} + \left.\frac{\partial}{\partial t}\left(\frac{\partial u}{\partial z}\right)\right|_{up} \delta z \tag{12}$$

For the bottom cell, if a log-layer distribution of velocity is assumed for fully developed turbulence, we have

$$\frac{\partial u}{\partial z} = \frac{u^*}{\kappa(z-h_0)} = \frac{u}{(z-h_0)\,\ln[(z-h_0)/z_0]} \tag{13}$$

where κ is the von Karman constant (0.41), u^* is the frictional velocity, $z_0 = k_s/30$, and k_s is the bottom roughness. Therefore, the local longitudinal acceleration at the cell centre is related to that at the u-point as follows:

$$\left.\frac{\partial u}{\partial t}\right|_{cc} = \left.\frac{\partial u}{\partial t}\right|_{up} + \frac{\delta z}{(z-h_0)\ln[(z-h_0)/z_0]} \left.\frac{\partial u}{\partial t}\right|_{up} \tag{14}$$

or

$$\frac{u_{cc}^{n+^*} - u_{cc}^n}{\Delta t} = \frac{u_{i,k}^{n+^*} - u_{i,k}^n}{\Delta t} + \frac{\delta z}{(z_k-h_0)\ln[(z_k-h_0)/z_0]} \frac{u_{i,k}^n - u_{i,k}^{n-1}}{\Delta t} \tag{15}$$

For surface computational cells, an inverse log-layer distribution of velocity is assumed for fully developed turbulence and we have

$$\frac{\partial u}{\partial z} = \frac{u^*}{\kappa(\eta - z)} \tag{16}$$

where $u^* = \sqrt{\tau_{wd}}/\rho$ and τ_{wd} is the wind shear stress in the longitudinal direction. Therefore,

$$\left.\frac{\partial u}{\partial t}\right|_{cc} = \left.\frac{\partial u}{\partial t}\right|_{up} + \frac{\delta z}{\kappa}\frac{\partial}{\partial t}\left(\frac{u^*}{\eta - z}\right) \tag{17}$$

or

$$\frac{u_{cc}^{n+^*} - u_{cc}^n}{\Delta t} = \frac{u_{i,k}^{n+^*} - u_{i,k}^n}{\Delta t} + \frac{\delta z}{\kappa \Delta t}\left(\frac{u_i^{*^n}}{\eta_i^n - z_k} - \frac{u_i^{*^{n-1}}}{\eta_i^{n-1} - z_k}\right) \tag{18}$$

Replacing the left-hand side of Equation (10) with the right-hand side of Equation (15) for the bottom computational u-cell and that of Equation (18) for the surface computational u-cell, the intermediate longitudinal velocity for the entire water column can be calculated from Equations (9) and (10). Once u^{n+^*} is determined, the intermediate vertical velocity and the intermediate free surface can be computed by considering the mass balance of the

computational c-cells and the mass balance of the water column of the each longitudinal grid. The resulting flux-based finite differences are

$$w_{i,k}^{n+^*} = \frac{1}{a_{zi,k+1/2}^n}(a_{zi,k-1/2}^n w_{i,k-1}^{n+^*} - \mathbf{F}_{i+1/2,k}^{n+^*} + \mathbf{F}_{i-1/2,k}^{n+^*} + v_{i,k}^{n+1/2}\Delta z_{i,k}^n \Delta x_i) \tag{19}$$

$$\Delta\eta_i^* = \eta_i^{n+^*} - \eta_i^n = -\frac{\Delta t\theta}{b_{\eta_i}^n \Delta x_i}(U_i^{n+^*} - U_{i-1}^{n+^*}) - \frac{\Delta t(1-\theta)}{b_{\eta_i}^n \Delta x_i}(U_i^n - U_{i-1}^n)$$

$$+ \frac{\Delta t}{b_{\eta_i}^n} \sum_{k=k_n}^{k_m^n} v_{i,k}^{n+1/2}\Delta z_{i,k}^n + \Delta t\, r^{n+1/2} \tag{20}$$

where $\mathbf{F}_{i-1/2,k}^{n+^*}$, calculated based on the u^{n+^*} distribution, is the water flux crossing the left face of the computational c-cell; $\Delta\eta_i^*(=\eta_i^{n+^*} - \eta_i^n)$ is the increment in free-surface elevation that is estimated from the intermediate velocity field, or $\Delta\eta_i^*$ is the difference between the intermediate free-surface and the free surface at the previous time step; $b_{n_i}^n$ is the average river width at the free surface of the ith grid; θ is a model parameter varying between 0 and 1 (fully explicit for $\theta = 0$ and fully implicit for $\theta = 1$); and $U_i^{n+^*}$ and U_i^n are the total water fluxes through the right face of the ith grid calculated using u^{n+^*} and u^n, respectively.

In the second step of the FSC method, the free-surface elevation is corrected by solving the following free-surface correction equation (see Reference [12] for details):

$$\eta_i^{n+1} - \eta_i^{n+^*} = \frac{g\theta^2\Delta t^2}{b_{\eta_i}^n \Delta x_i}\left(\mathscr{A}_{i+1/2}\frac{\Delta\eta_{i+1} - \Delta\eta_i}{\Delta x_{i+1/2}} - \mathscr{A}_{i-1/2}\frac{\Delta\eta_i - \Delta\eta_{i-1}}{\Delta x_{i-1/2}}\right) \tag{21}$$

where $\Delta\eta_i(=\eta_i^{n+1} - \eta_i^n)$ is the final increment of the free surface over the time step Δt and $\mathscr{A}_{i+1/2}$ is the cross-section area at the right face of the longitudinal grid (the sum of wetted areas of right faces for grid cells with the longitudinal grid index i). Equation (21) can be re-arranged as follows:

$$-R_w\Delta\eta_{i-1} + (1 + R_w + R_e)\Delta\eta_i - R_e\Delta\eta_{i+1} = \Delta\eta_i^* \tag{22}$$

where

$$R_w = \frac{g\theta^2\Delta t^2}{\Delta x_i \Delta x_{i-1/2}}\frac{\mathscr{A}_{i-1/2}}{b_{\eta_i}^n}, \qquad R_e = \frac{g\theta^2\Delta t^2}{\Delta x_i \Delta x_{i-1/2}}\frac{\mathscr{A}_{i+1/2}}{b_{\eta_i}^n} \tag{23}$$

Equation (22) is a tri-diagonal system and can be easily solved using the Thomas Algorithm. After the final free-surface location is found, the final longitudinal momentum equation can be solved from the following velocity-correction equation [12]:

$$u_{i,k}^{n+1} = u_{i,k}^{n+^*} - g\theta\Delta t\frac{\partial\Delta\eta}{\partial x} \tag{24}$$

The final vertical velocity field is calculated from the following flux-based finite difference equation that guarantees the mass conservation for each computational c-cell:

$$w_{i,k}^{n+1} = \frac{1}{a_{zi,k+1/2}^n}(a_{zi,k-1/2}^n w_{i,k-1}^{n+1} - \mathbf{F}_{i+1/2,k}^{n+1} + \mathbf{F}_{i-1/2,k}^{n+1} + v_{i,k}^{n+1/2}\Delta z_{i,k}^n \Delta x_i) \tag{25}$$

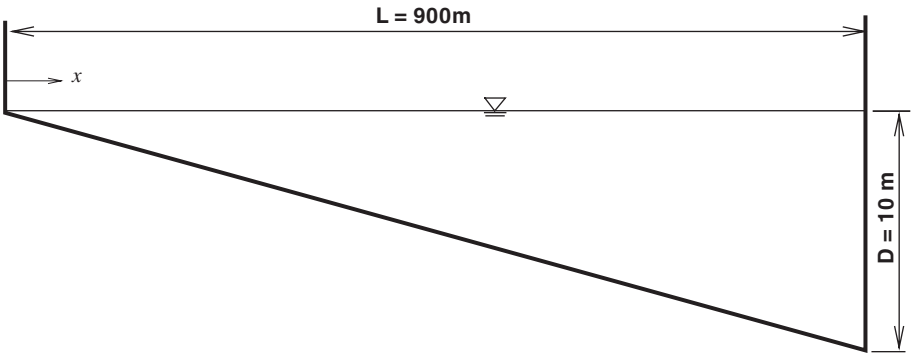

Figure 5. A triangular basin with a constant width.

where $\mathbf{F}^{n+1}_{i-1/2,k}$ is the water flux crossing the left face of the computational c-cell and is calculated using the final longitudinal velocity distribution.

For the transport equation, the flux-based finite difference equation is derived from the mass balance of the material for the computational c-cell. With an implicit discretization of the vertical diffusion term, the resulting flux-based finite difference equation takes the following form

$$\frac{V^{n+1}_{i,k}c^{n+1}_{i,k} - V^{n}_{i,k}c^{n}_{i,k}}{\Delta t} = -F^{n}_{xi+1/2,k} + F^{n}_{xi-1/2,k} - F^{n}_{zi,k+1/2} + F^{n}_{zi,k-1/2} + F^{n+1/2}_{yi,k} + F^{n+1/2}_{ri,k}$$
$$+ \left(a_x B_h \frac{\partial c^n}{\partial x}\right)_{i+1/2,k} - \left(a_x B_h \frac{\partial c^n}{\partial x}\right)^{n}_{i-1/2,k}$$
$$+ \left(a_z B_v \frac{\partial c^{n+1}}{\partial z}\right)_{i,k+1/2} - \left(a_z B_v \frac{\partial c^{n+1}}{\partial z}\right)_{i,k-1/2} \tag{26}$$

where V is the volume of the cell, $F^{n}_{xi+1/2,k}$ and $F^{n}_{zi,k+1/2}$ are advective fluxes through the right and top faces of the cell; and $F^{n+1/2}_{yi,k}$ and $F^{n+1/2}_{ri,k}$ are fluxes from the tributaries and from the atmosphere ($F^{n+1/2}_{ri,k}$ is always zero for cells other than the surface cell).

5. TESTS OF BOTTOM TREATMENT METHODS

5.1. An initial value problem

The initial value problem is a seiche oscillation in a triangular basin with a constant width (Figure 5) and a constant density. The right-angled basin has the following depth profile:

$$d(x) = \frac{D}{L}x \tag{27}$$

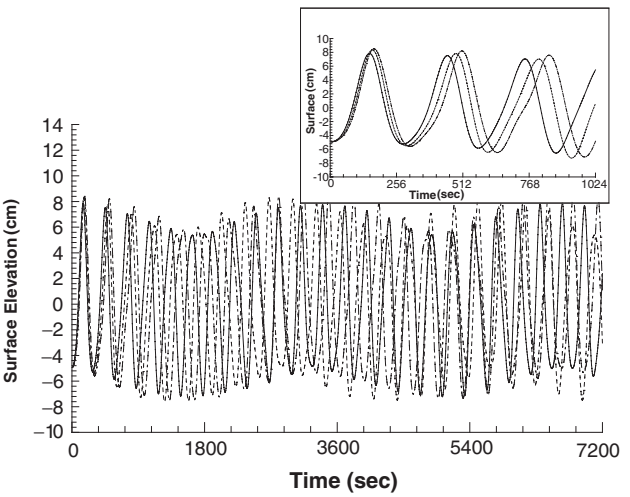

Figure 6. Comparison of the simulated surface elevations at $x = 50\,\mathrm{m}$ of the triangular basin using the three different bottom treatment methods (solidline is piecewise linear bottom, dashed line is partial cell and dash–dotted line is full cell). The small inset is a zoom-in for the first 1024 s. The aspect ratio of the grid cell is 0.004.

where d is the water depth, x is measured from left to right, D is the maximum depth of the basin and L is the basin length. The seiche oscillation is generated by an initial surface set-up with the following sinusoidal function:

$$\eta = 5 \sin\left(\frac{2x - L}{2L}\pi\right) \tag{28}$$

where the surface elevation η is in cm.

In the initial value problem, $D = 10\,\mathrm{m}$ and $L = 900\,\mathrm{m}$. When the LAMFE model was applied to simulate the oscillation, a constant vertical spacing of $\Delta\zeta = 0.4\mathrm{m}$ and a constant longitudinal spacing of $\Delta x = 100\,\mathrm{m}$ were used. All three topography treatment methods (full cells, partial cells and the piecewise linear bottom) were tested and model results were compared to observe the responses of the model to various treatment methods. Frictions at the bottom and the sidewall were set to zero in simulating the seiche oscillation case. Eddy viscosities used for both the vertical and longitudinal directions were constant and very small ($A_h = 5\,\mathrm{cm^2\,s^{-1}}$ and $A_v = 1\,\mathrm{cm^2\,s^{-1}}$).

Figure 6 shows simulated surface elevations at $x = 50\,\mathrm{m}$ using the three bottom treatment options. The solid line in Figure 6 is the simulated surface using the piecewise linear bottom treatment. Dashed and dotted lines are simulated water surfaces using the full cell and partial cell options, respectively. From Figure 6, it can be seen that simulated surface elevations using different bottom treatment methods are quite different. While the simulated surface elevations vary in a similar way for all three simulations, their differences become larger as time goes on. This is mainly due to the fact that the simulated fundamental wave periods are different for the three bottom topography treatments. The small inset in Figure 6 shows the first 1024 s of the model results. The differences in wave speed can be clearly seen.

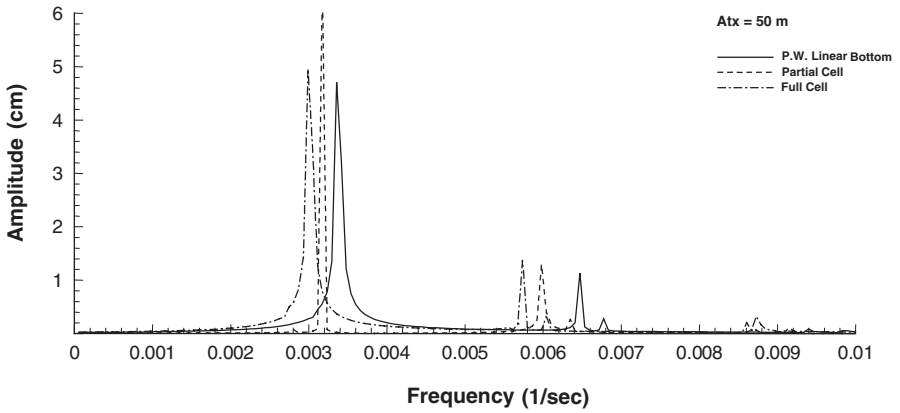

Figure 7. Comparison of FFT results for simulated surface elevations at $x = 50$ m of the triangular basin using the three different bottom treatment methods (solidline is piecewise linear bottom, dashed line is partial cell and dash–dotted line is full cell).

For a triangular basin with a constant width, the analytical solution for the period of the first mode oscillation takes the following form [14]:

$$T_1 = 1.64 \frac{2L}{\sqrt{gD}} \tag{29}$$

where T_1 is the fundamental wave period. For the triangular basin studied here, the analytical value of T_1 can be calculated and has a value of 298.05 s. Simulated fundamental wave periods can be obtained by performing fast Fourier transform (FFT) to simulated surface elevations. Figure 7 shows FFT results for simulated surface elevation at $x = 50$ m. The solid line is the result of the piecewise linear bottom option and has peak values at a frequency of $0.003357\,\mathrm{s}^{-1}$. This corresponds to a wave period of 297.89 s and is very close to the analytical T_1 of 298.05 s. The dashed and dash–dotted lines are results using the partial cell and full cell options, respectively. The corresponding first mode periods for these two runs are 315.06 and 334.34 s, respectively. Compared to a relative error of just 0.054% for the piecewise linear bottom treatment, the relative errors for the partial cell and full cell treatments are 5.707 and 12.176%, respectively. Obviously, the full cell option is not a good choice for this kind of initial problem with a variable depth. Even the partial cell option is problematic with a relative error over 5%.

The test case was also simulated using a different Cartesian grid system with a constant vertical spacing of $\Delta\zeta = 1.0$ m and a constant longitudinal spacing of $\Delta x = 45$ m. Obviously, the aspect ratio of the grid cell ($\Delta\zeta/\Delta x$) in the second grid system is much larger than that of the first grid system. As a result, both the full cell option and the partial cell option have a worse fitness of the bottom than those of the first grid system do. In Figure 8, simulated surface elevations at $x = 67.5$ and 832.5 m are shown with solid and dashed lines, respectively. While Figure 8(a) shows model results using the piecewise linear bottom options, Figures 8(b) and 8(c) show model results using the partial cell option and the full cell option, respectively. It is apparent that due to a larger aspect ratio, model results using partial or full cells differ further more from those using the piecewise linear bottom. Some higher mode oscillations can be

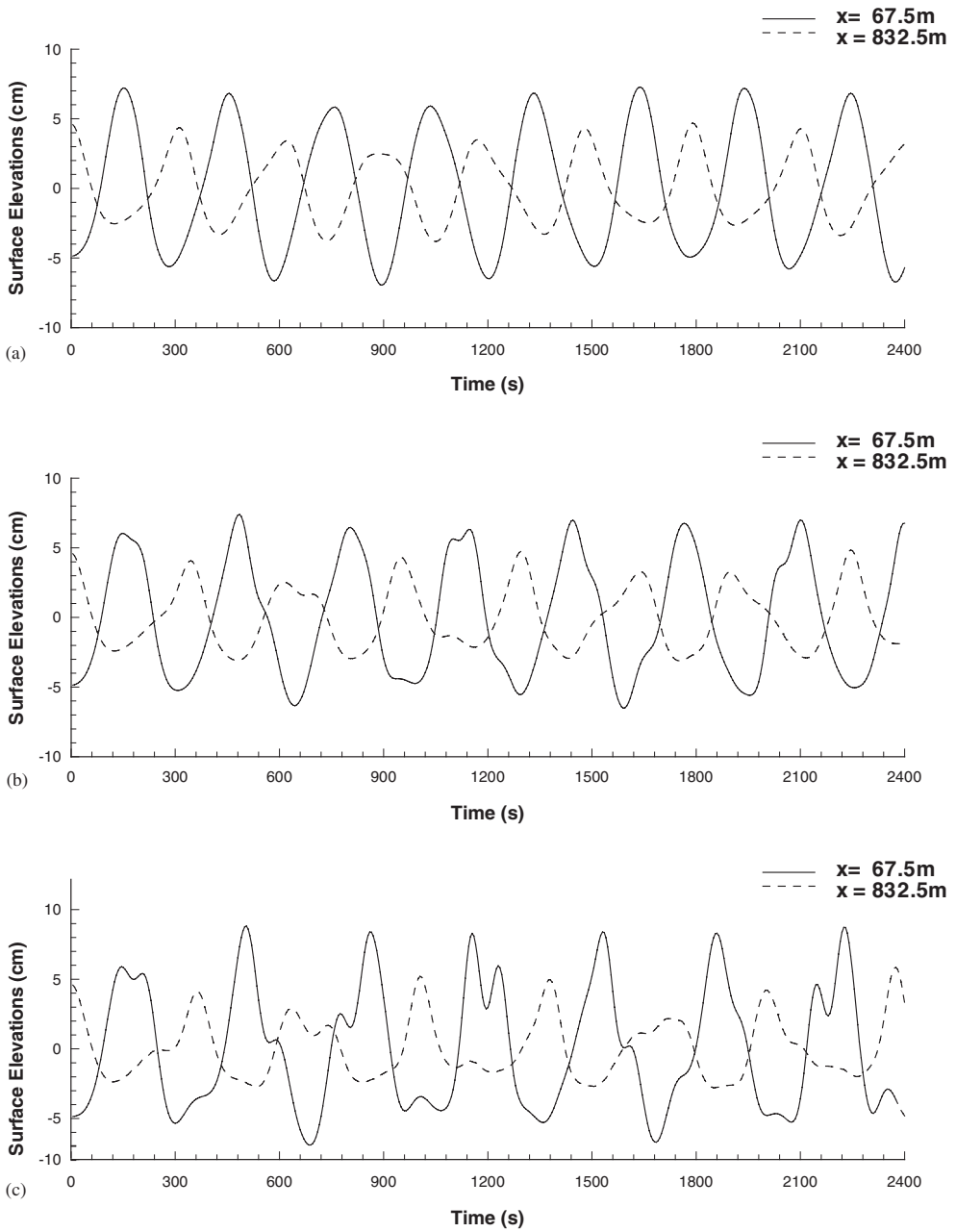

Figure 8. Comparison of the simulated surface elevations at $x = 67.5$ and $x = 832.5$ m of the triangular basin using the piecewise linear bottom (a), partial cells (b) and full cells (c). The aspect raton of the grid cell is 0.0222.

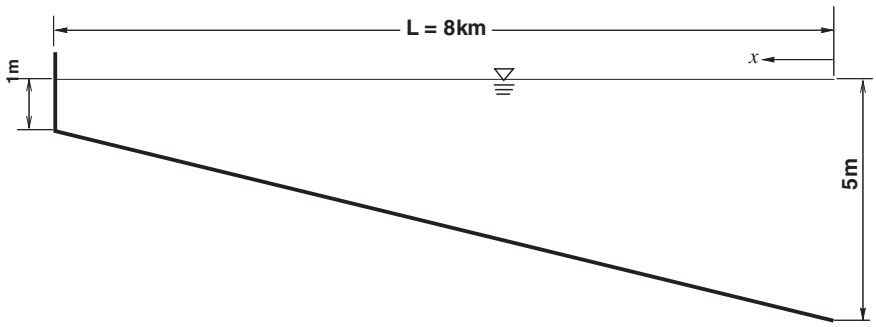

Figure 9. A sloping open channel with one open end and one closed end.

seen in model results using the partial cell option. In model results using the full cell option, these higher mode oscillations are further enhanced. An FFT analysis similar to that shown in Figure 7 was conducted for simulated surface elevations at $x = 67.5$ m using the three bottom treatment methods. The first mode periods are 297.89, 321.25 and 341.33 s for the piecewise linear bottom option, the partial cell option and the full cell option, respectively. Since the fitness of the bottom is not affected by the aspect ratio of the grid cell when the piecewise linear bottom is used, the first mode period remains 297.89 s, the same as that in the first grid system with a relative error of just 0.054%. However, the relative errors of the first model period for the partial and full cell options now become 7.784 and 14.521%, respectively, and both are at least 2% larger than the relative errors for the two bottom treatment methods using the first grid system.

5.2. A boundary value problem

The boundary value problem used to test the responses of the LAMFE model to various bottom treatment methods is a co-oscillating wave entering a sloping channel (Figure 9) that has a length of 8 km and a width of 100 m. One end of the channel is closed, while the other is open. The water depth decreases linearly from 5 m at the open end to 1 m at the closed end. The density in the channel is constant. The boundary condition at the open end is specified by a small amplitude wave with an amplitude of 2 cm and a wave period of 1 h.

The analytical solution for this boundary value problem can be found in References [15, 16]. It can also be easily derived by superimposing the incident wave with waves reflected from the closed end and along the channel due to a decease in water depth [12]

$$h = h_{\mathrm{i}} + h_{\mathrm{rx}} + h_{\mathrm{l}} \tag{30}$$

where h_{i} is the incident wave, and h_{rx} and h_{l} are reflected waves along the channel and from the closed end, respectively. The incident wave takes the following form [17, 18]:

$$h_{\mathrm{i}} = a\mathrm{e}^{\mathrm{j}(\lambda+\omega t)} \tag{31}$$

where $j = \sqrt{-1}$, $\lambda = \int_0^x k\,\mathrm{d}x$, $k = \omega/\sqrt{gh}$; the x-co-ordinate is from right to left; and a is the amplitude of the incident wave and can be calculated from the following equation:

$$a\sqrt{gk} = a_0\sqrt{gk_0} \tag{32}$$

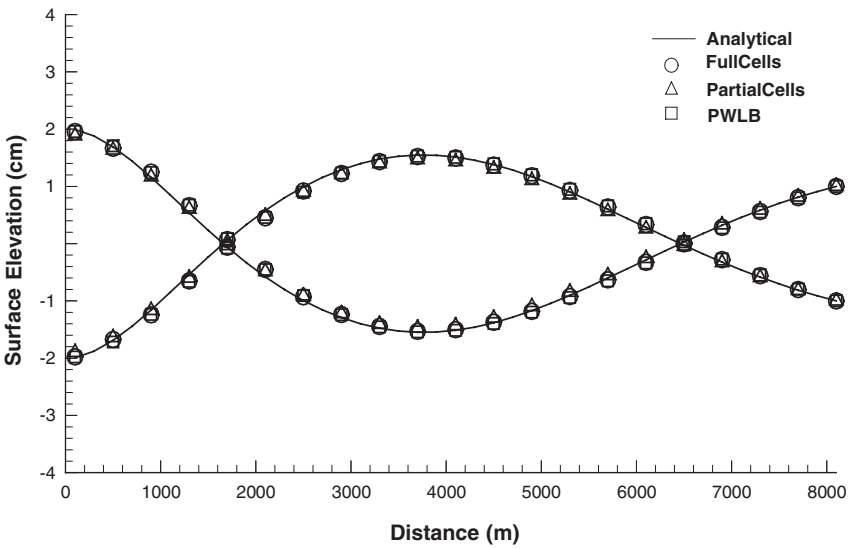

Figure 10. Comparison of simulated free-surface elevations using the three bottom treatment methods with analytical solutions for a co-oscillating wave case in a sloping channel. Solid lines are analytical solutions, squares are model results using a piecewise linear bottom (PWLB). Circles and triangles are those using the partial cell and full cell options, respectively.

where a_0 is the incident wave amplitude at the open end of the channel. Waves reflected along the channel can be expressed as follows:

$$h_{\mathrm{rx}} = R(x) a \mathrm{e}^{\mathrm{j}(\lambda - \omega t)} \tag{33}$$

where R is the reflection coefficient, which, to the order of the bottom slope, is [18]

$$R(x) \approx -\frac{1}{2} \int_0^x \left[\frac{\mathrm{d}}{\mathrm{d}x} \ln(kh) \right] \mathrm{e}^{2\mathrm{j}\lambda} \, \mathrm{d}x \tag{34}$$

The reflected wave from the wall at the closed end is

$$h_{\mathrm{l}} = [1 - R(L)] a \mathrm{e}^{\mathrm{j}(\lambda - \omega t)} \tag{35}$$

When the LAMFE model was applied to this boundary value problem, a uniformly distributed grid system was used with a vertical spacing of $\Delta\zeta = 0.5\,\mathrm{m}$ and a longitudinal spacing of $\Delta x = 400\,\mathrm{m}$. The model was run from the cold start by assuming that the water in the basin is still at $t = 0$. The model was run for 200 wave cycles with three different bottom treatment methods. The bottom and sidewall frictions were set to zero for the model runs. The eddy viscosity terms were omitted. Model results show that a dynamic steady state was normally achieved after less than 15 cycles. Therefore, the initial disturbances disappear after 15 cycles and the steady-state model results are the numerical solutions for the boundary value problem.

Figure 10 shows the comparison of analytical solutions with model results using the three bottom treatment methods. It compares two instantaneous free surfaces computed from the model with the analytical free surfaces. The solid lines are analytical solutions, while the symbols are numerical model results. Simulated free surfaces using the piecewise linear bottom

are plotted with squares (□), while those using the full cell and partial cell options are drawn with circles (○) and triangles (△), respectively. It can be seen that although the piecewise linear bottom still yields the best model results, the differences among simulated free surfaces using different bottom treatment methods are small and all three methods work very well for this co-oscillating wave case. The root-mean-square (RMS) errors for the piecewise linear bottom, partial cells and full cells are about 1.53, 2.49 and 3.38%, respectively, of the wave amplitude at the open end.

5.3. A barotropic case

In has been mentioned in Section 1 that although a σ-co-ordinate model can fit the topography nicely, it has problems associated with pressure gradient errors and increased numerical diffusions for areas with steep bottom slopes [3, 4]. Huang and Spaulding [19] investigated the artificial diffusion problem of a σ-co-ordinate model in a closed sloping basin with a slope of 0.03. At $t = 0$, the water in the basin was still with a stable vertical density stratification (salinity at $t = 0$ varied from 31 ppt at the bottom to 13 ppt at the free surface). After a simulation period of 30 days, a strong artificial baroclinic circulation was generated with a totally different salinity distribution from that at $t = 0$. The difference between the initial salinity field at $t = 0$ and the predicted salinity field at the end of the 30-day simulation using a σ-co-ordinate model could be as large as over 5 ppt in the basin. To confirm that the use of the piecewise linear bottom in the LAMFE model does not cause any increased numerical diffusions in areas with steep bottom slopes, a barotropic case in a symmetric triangular basin was tested in this study to evaluate the performance of the piecewise linear bottom. As shown in Plate 1, the symmetric triangular basin has a length of 400 m and a maximum depth of 6 m in the middle of the basin. The slope of the basin is 0.03, the same as that in the test case of Huang and Spaulding [19]. At $t = 0$, salinity in the basin varies only in the vertical direction, from about 30 ppt at the lowest point of the basin to about 12 ppt at the free surface. The simulation domain was discretized using uniform grid cells that have a vertical spacing of $\Delta\zeta = 0.6$ m and a longitudinal spacing of $\Delta x = 20$ m. The model was run for a simulation period of 30 days (720 h) using the piecewise linear bottom. Plate 1(a) shows the initial salinity and velocity distributions in the triangular basin. Simulated salinity and velocity distributions at $t = 720$ h are shown in Plate 1(b). It can be seen that both Plates 1(a) and 1(b) are identical. No artificial baroclinic circulation was generated during the model run.

5.4. A real riverine estuary case

The LAMFE model was used to simulate hydrodynamics in the Lower Hillsborough River located in Tampa, Florida using the three topography treatments. The simulation domain is from the City of Tampa Dam to Platt Street (Figure 11) and has a total length of about 16 km. Measured real-time data at the upstream and downstream boundaries were used as boundary conditions. Model results were compared to observe the responses of the LAMFE model to the three topography treatment methods.

Figure 12 shows the z-level grid system used for the model runs. Thirty-two grids ranging from 300 to 840 m in length were used along the river and 16 vertical grids were used to resolve the depth with a vertical spacing varying from 30 to 50 cm. The thick solid line indicates the piecewise linear bottom used in the simulation. Figure 13 shows comparisons

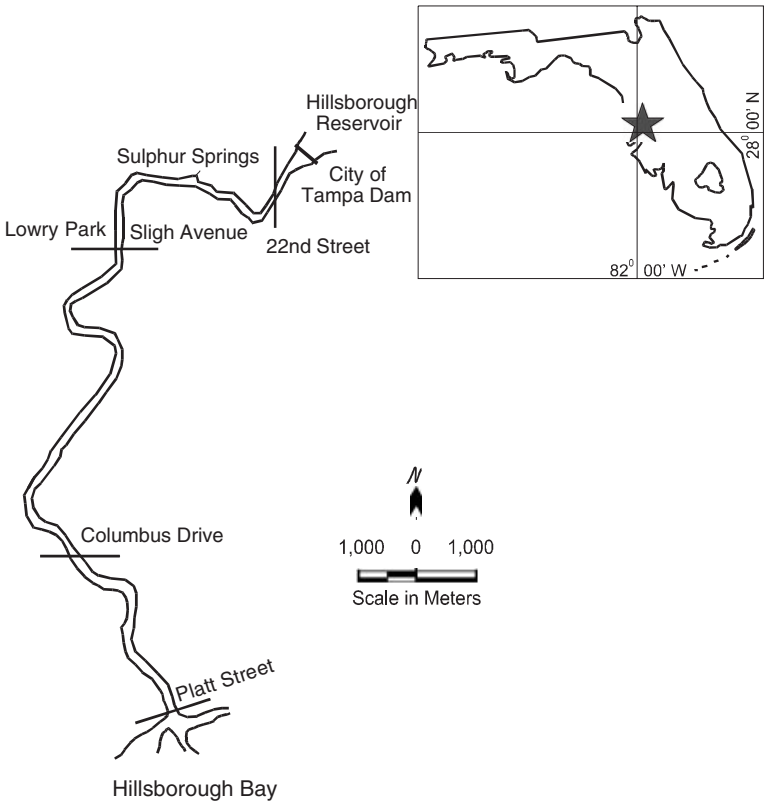

Figure 11. The Lower Hillsborough River, Tampa, FL, U.S.A.

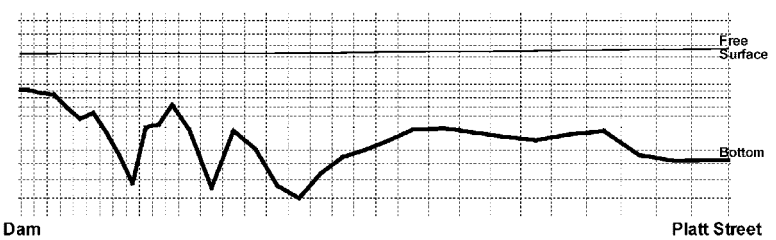

Figure 12. A z-level grid system for the Lower Hillsborough River, Florida with a piecewise linear bottom.

of simulated time series of surface elevation at Sligh Avenue and mid-depth salinity at Columbus Drive (Figure 11) with those of measured real-time data, which are drawn as solid lines. Dashed lines in Figure 13 indicate model results with the piecewise linear bottom, while dash–dotted lines and dash–dot–dotted lines indicate those with partial cells and full cells, respectively. It can be seen from the figure that simulated surface elevations agree very well with measured data, regardless of which bottom treatment method is used. The RMS

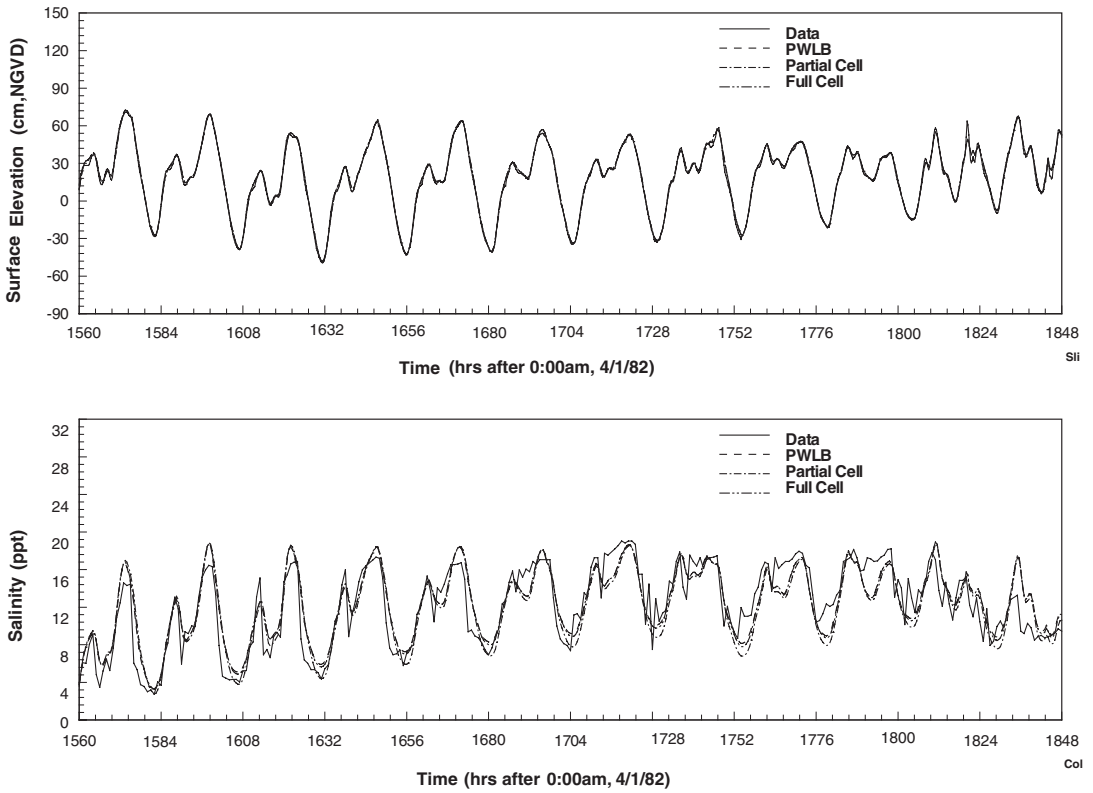

Figure 13. Comparison of simulated free surfaces (top, at Sligh Avenue) and salinity (bottom, at the mid-depth of Columbus Drive) in the Lower Hillsborough River, Florida using the three bottom treatment methods with measured data.

errors between simulated and measure surface elevation are only about 1.07, 1.98 and 2.53 cm for the piecewise linear bottom, partial cells and full cells, respectively. Except during the low tide, differences among simulated salt concentrations using three different bottom treatments are generally insignificant in comparison to the differences between measured salinity and simulated salinity using either one of the three methods. This suggests that factors other than the topography fitting (e.g. freshwater inflows, bathymetry data, measured salinity at the downstream open boundary, etc.) may contribute major errors to the model results. The RMS errors between simulated and measured salinity for the piecewise linear bottom, partial cells and full cells are 1.85, 1.98, and 2.02 ppt, respectively. Although the elevation of the riverbed varies significantly along the river, model results using different topography treatment methods do not exhibit significant differences for this riverine estuary that is mainly driven by the tide and salinity at the downstream boundary and the freshwater inflow at the upstream boundary. Since a relatively fine resolution was used to discretize the water column, the fact that no significant differences were observed in model results using different bottom treatment methods suggests that for this dominantly boundary value problem, the requirement for terrain-following may not be very critical if an appropriate vertical spacing is used.

6. CONCLUSIONS

A piecewise linear bottom has been used in a laterally averaged, 2D hydrodynamic model named LAMFE. The use of the piecewise linear bottom results in a hybrid z-level model that is capable of fitting the bottom topography, but does not possess the usual drawbacks normally seen in a stretched co-ordinate model such as a σ-level model. Since computational cells are not necessarily the same as the grid cells and their side views are not necessarily rectangular, flux-based finite difference equations are derived and used in the model. The use of flux-based finite difference equations guarantees that the mass conservation is satisfied both locally and globally. Additional coding effort due to the use of computational cells is only minor.

The LAMFE model was used to simulate an initial value problem and a boundary value problem to evaluate the responses of the model to different topography treatments. The initial value problem is a seiche oscillation in a triangular basin, while the boundary value problem is a co-oscillating wave in a channel with a bottom slope of 1/2000. Responses of the model to full cells, partial cells and the piecewise linear bottom were investigated for the two wave cases. To verify that the use of the piecewise linear bottom can avoid the numerical diffusion problem often seen in a σ-co-ordinate model for areas with steep bottom slopes, the piecewise linear bottom option for the topography treatment was tested with a barotropic case in a symmetric triangular basin. The model was then applied to the Lower Hillsborough River, FL, U.S.A. to compare the differences among simulated results using the three topography treatment methods.

Model tests show that the piecewise linear bottom allows a z-co-ordinate model to fit the bottom topography, yet does not possess any problems associated with pressure gradient errors and increased numerical diffusions. This can be clearly seen from the model results for the barotropic test case. The model was run for a simulation period of 30 days, but no artificial baroclinic circulation was generated, indicating that the hybrid z-level model presented here is able to retain the advantage of a traditional z-level model. In all test cases, model results using the piecewise linear bottom are always better than those using partial cells, which are better than those using full cells. It was found that fitting the topography is especially important for initial value problems. With a larger aspect ratio of the grid cell, model results using full cells or partial cells contain larger errors due to the poor fitness of the bottom topography. For the boundary value problem and the salinity transport process in the Lower Hillsborough River, the piecewise linear bottom yields better model results than the partial cell option or the full cell option does. Nevertheless, the necessity for topography-fitting may not be very critical in predicting the free-surface elevation and the mid-depth salinity, provided that the vertical spacing is fine enough to appropriately describe river cross-sections. Future research using various resolutions for the water column discretization need to be conducted to study the differences between model results using a staircase bottom and those using a piecewise linear bottom and to reveal how model results using the staircase bottom (full cells or partial cells) will approach those using the piecewise linear bottom as the vertical resolution increases.

Unlike a σ-co-ordinate model that has to set a minimum water depth in the simulation domain to ensure that the vertical spacing does not become zero, the piecewise linear bottom does allow the water depth to go to zero (see the first and the third test cases where two different triangular basins were used for model testing.) This is another advantage that the piecewise linear bottom has over a σ-co-ordinate model. In many model applications in the

area of coastal environmental engineering, allowing the water depth to go to zero is very important, because many ecological processes only occur in very shallow areas where the depth approaches zero.

REFERENCES

1. Sheng YP, Butler HL. A three-dimensional numerical model of coastal, estuarine, and lake currents. In *Proceedings*, *1982 Army Numerical Analysis and Computers Conference*, *U.S. Army Research Office Report* No. 82-3, Washington, DC, 1982; 531–574.
2. Blumberg AF, Mellor GL. A description of a three-dimensional coastal ocean circulation model. *Three-Dimensional Coastal Ocean Models*. American Geophysical Union, 1987; 116.
3. Sheng YP, Lee HK, Wang KH. On numerical strategies of estuarine and coastal modeling. In *Estuarine and Coastal Modeling*, Spaulding ML (ed.), *Proceedings of the Conference*. ASCE: New York, 1989; 291–301.
4. Mellor GL, Oey LY, Ezer T. Sigma co-ordinate pressure gradient errors and the seamount problem. *Journal of Atmospheric and Oceanic Technology* 1998; **15**(5):1122–1131.
5. Leendertse JJ, Liu SK. A three-dimensional model for estuaries and tidal seas. II Aspects of computation. *Technical Report* R-1764-OWRT, Rand Corporation, 1975.
6. Casulli V, Cheng RT. Semi-implicit finite difference methods for three-dimensional shallow water flow. *International Journal for Numerical Methods in Fluids* 1992; **15**:629–648.
7. Chen X. Simulating salinity distribution in the Lower Hillsborough River with a laterally averaged two-dimensional hydrodynamic model. *Technical Report*, Southwest Florida Water management District, Brooksville, FL, 1997.
8. Chen X, Flannery MS. Use of a hydrodynamic model for establishing a minimum freshwater flow to the Lower Hillsborough River. In *Estuarine and Coastal Modeling*, Spaulding ML, Blumberg AF (eds), *Proceedings of 5th International Conference*. ASCE: New York, 1998; 663–678.
9. Chen X, Flannery MS, Moore DL. Response times of salinity in relation to changes in freshwater inflows in the Lower Hillsborough River, Florida. *Estuaries* 2000; **23**(5):735–742.
10. Bijvelds MDJP, van Kester J, Stelling GS. A comparison to two 3D shallow water models using sigma-co-ordinates and *z*-co-ordinates in the vertical direction. In *Estuarine and Coastal Modeling*, Spaulding ML, Lee Butler H (eds), *Proceedings of 6th International Conference*. ASCE: New York, 1999; **130**:147.
11. Pacanowski RC, Gnanadesikan A. Transient response in a *z*-level ocean model that resolves topography with partial cells. *Monthly Weather Review* 1998; **126**(10):3248–3270.
12. Chen X. An efficient finite difference scheme for simulating hydrodynamics in narrow rivers and estuaries. *International Journal for Numerical Methods in Fluids* 2003; **42**(3):233–247.
13. Chen X. Responses of a hybrid *z*-level model to various topography treatment methods for a boundary value problem and an initial value problem. In *Estuarine and Coastal Modeling*, Spaulding ML (ed.), *Proceedings of the 7th International Conference*. ASCE: New York, 2001; 614–627.
14. Wilson BS. Seiches. In *Advances in Hydroscience*, Ven Te Chow (ed.), vol. 8. Academic Press: New York, 1972.
15. Lamb H. *Hydrodynamics*. Dover: New York, 1945.
16. Lynch DR, Gray WG. Analytical solutions for computer flow model testing. *Journal of the Hydraulics Division*, *Proceedings of the ASCE* 1978; **104**(HY10):1409–1428.
17. Kajiura K. On the partial reflection of water waves passing over a bottom of variable depth. *Proceedings of the Tsunami Meetings 10th Pacific Science Congress*, IUGG Monograph, vol. 24, 1961; 206–234.
18. Mei CC. *The Applied Dynamics of Ocean Surface Waves*, Advanced Series on Ocean Engineering, vol. 1. World Scientific: Singapore, 1989.
19. Huang WR, Spaulding M. Reducing horizontal diffusion error in σ-co-ordinate coastal ocean models with a second-order Lagrangian-interpolation finite-difference scheme. *Ocean Engineering* 2002; **29**:495–512.

